A model-based approach for geometric correction of optical satellite images

Report from SNOWTOOLS WP 220

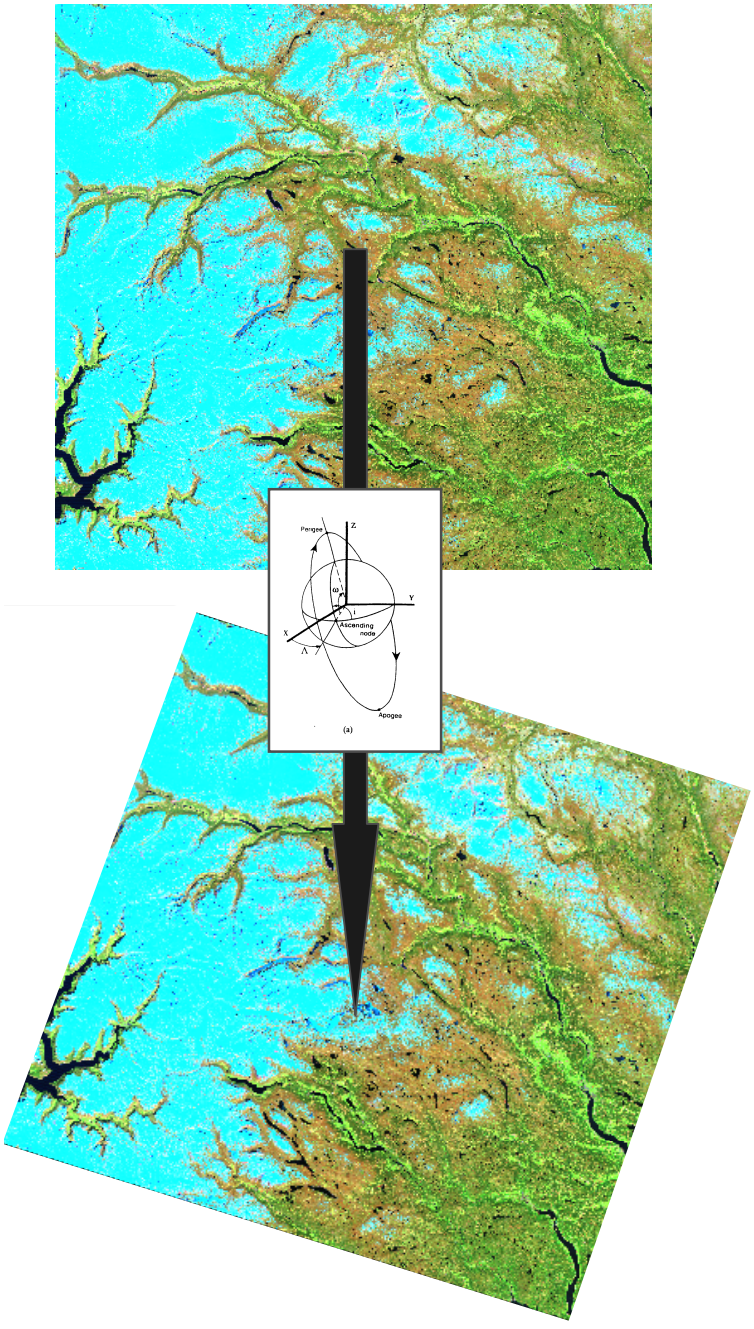

Report no. 932

Ragnar Bang Huseby
Rune Solberg

October 1998

Norsk Regnesentral
ANVENDT DATAFORSKNING

Rapport/Report

Tittel/Title: A model-based approach for geometrical correction of optical satellite images

Dato/Date: October
År/Year: 1998
ISBN: 82-539-0415-0
Publikasjonsnr.: Report no. 932
Publication no.:

Forfatter/Author: Ragnar Bang Huseby, Rune Solberg

Sammendrag/Abstract:
In this report, we describe a method for geometric correction of satellite images generalizing a method developed for NOAA AVHRR images. The method is based on modeling the imaging process, including satellite orbital modeling. We also present an approach for automatic detection of ground control points based on matching of a near-infrared band with watermasks. The methods have been tested on two images: a system-corrected Landsat TM image with pixel size 30 m $\times$ 30 m, and an image with pixel size 240 m $\times$ 240 m (similar to EOS MODIS) derived from the system-corrected Landsat TM image. The detection procedure gave satisfying results. Using the correction method we obtained root mean square errors of 4.3 pixel units and 0.9 pixel units, respectively, on a set of ground control points. The results are satisfying for EOS MODIS, however, higher accuracy is desired for Landsat TM, and improvements are suggested.

Emneord/Keywords: geometrisk korreksjon, geokoding, kontrollpunkter/
geometric correction, geocoding, ground control points

Tilgjengelighet/Availability: åpen/open

Prosjektnr./Project no.: 900402

Satsningsfelt/Research field: fjernmåling/remote sensing

Antall sider/No. of pages: 24

Norsk Regnesentral / Norwegian Computing Center
Gaustadalléen 23, Postboks 114 Blindern, 0314 Oslo, Norway
Telefon 22 85 25 00, telefax 22 69 76 60

TABLE OF CONTENTS

1. Introduction

The raw data obtained by a remote sensing system is seldom adequate for high-precision applications due to various distortions. The distortions can be divided into geometric and radiometric distortions. In this report, we consider only geometric errors, and the goal of our work is to correct satellite images for such errors.

The sources of geometric distortions include sensor effects, platform effects, object effects, and atmospheric effects. We will briefly mention some examples of distortions. In a raw image the pixel size on the ground is not constant since it varies with the scanning angle. If the velocity of the satellite relative to the ground is not constant, the distance between two neighboring scan lines is not constant. Further distortions are caused by the fact that the attitude of the satellite varies with time. The Earth's rotation implies that the scan lines are shifted relative to each other in the direction approximately perpendicular to the track. A point at a high altitude will appear to lie further from nadir than a point at a low altitude with the same latitude and longitude for oblique viewing directions. In addition, atmospheric refraction may cause geometrical distortions. Some of the errors are systematic, while some of the errors occur more or less randomly.

By geometric correction, an image is derived from the raw image such that it has the same geometry as a reference image or a well-defined map projection. For each pixel in the corrected image, we want to determine a mapping to the raw image. In our approach, we attempt to account for some of these effects that cause distortion. We feel that prior knowledge about the situation of the image acquisition should be used as far possible. In addition, it is necessary to update this knowledge by using a set of ground control points which location in the image and on the scene is known.

In Section 2, we describe briefly an algorithm for geometric correction that has been used at the Norwegian Computing Center. In Section 3, we present a generalization of this algorithm. Section 4 contains a description of a method for detecting ground control points automatically. The Landsat TM data, on which the algorithms are tested, are described in Section 5. The correction procedure is also tested on an image with pixel size 240 m $\times$ 240 m obtained from the system-corrected Landsat image by using a resampling procedure. This is done in order to predict the accuracy of the correction procedure on bands 1-2 from the EOS Moderate Resolution Imaging Spectrometer (MODIS) since these bands have approximately the same resolution. The experiments are reported in Section 6, and a discussion with conclusions are given in Section 7.

2. An algorithm for geometric correction of satellite images

The algorithm for geometric correction developed in this project is based on an algorithm previously developed at the Norwegian Computing Center, [2]. The previous algorithm is adapted for data from the Advanced Very High Resolution Radiometer (AVHRR) on board the NOAA series of satellites. In the method, which is a modification of the one presented by Moreno and Meliá in [1], a Keplerian orbital model for the satellite motion is considered as a reference model, and estimates of orbital elements are given as input from ephemeris data. The orbital elements are semi-major axis, inclination, eccentricity, argument of perigee, longitude of ascending node, and mean anomaly, [1]. Fig. 1 shows the definition of inclination, argument of perigee, and longitude of ascending node. A number of ground control points (GCPs) are then introduced to improve the estimates of two of the orbital elements. This is explained in the following steps.

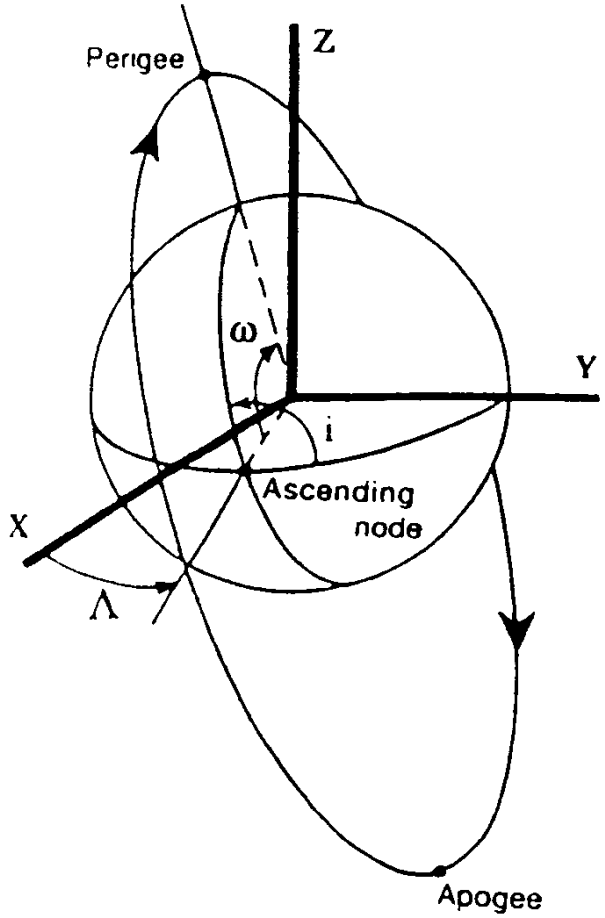

Fig. 1. Orbital parameters for a simplified Keplerian elliptic orbit. Definition of three angles that determine the orbit plane and orientation: inclination (i), perigee argument (ω), longitude of ascending node (Λ). (The figure is taken from [1].)

In the first step, the estimated longitude of ascending node is adjusted. Using geometrical relationships involving the GCPs, lower and upper bounds for the longitude of the ascending node are obtained. The updated estimate is taken to be the average of these bounds. In the second step, the mean anomaly is adjusted. This is done by comparing the actual line number (in the raw image) of each GCP with the nominal line number (in the raw image) predicted from the orbital model.

The algorithm also corrects for attitude angle variations. Two vectors define the attitude geometry: the vector normal to the scanning plane and the vector that defines the instantaneous viewing direction of the first pixel of each line, see Fig. 2. The components of these two vectors are modeled as second degree polynomials in time. The coefficients of the polynomials are estimated using information about the position and the velocity of the satellite and the location of the GCPs in the raw image and in the scene.

Having described the position of the satellite and the image geometry as a function of time, the time instant and, hence, the line and the pixel number in the raw image corresponding to the geographical coordinates of a given point in the scene can be calculated. A bisection method does this. In this way we obtain a correspondence between pixels in the raw image and pixels in the corrected image. The pixel value in the corrected image is then set to a value of the corresponding position in the raw image determined by a resampling technique.

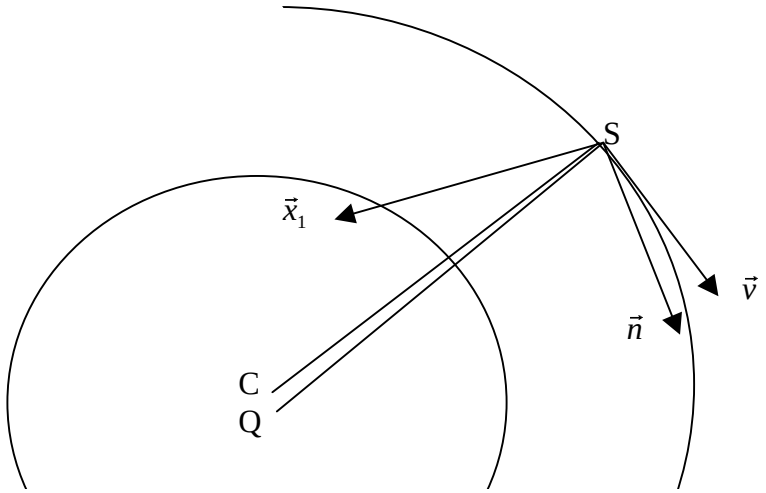

Fig. 2. Fundamental vectors.
S is the satellite position. C is the center of Earth. The vector from S to Q is the nominal nadir direction. $\vec{v}$ is the velocity of the satellite. $\vec{n}$ is the normal to the scanning plane. $\vec{x}_1$ is the viewing-direction vector of the first pixel of the corresponding scan line.

3. Generalization of the algorithm

The correction algorithm adapted for NOAA/AVHRR assumes that just one line is acquired at a time. In addition, the pixels on a scan line are distributed according to a certain pattern. More specifically, the size of the viewing angle corresponding to a given pixel in the raw image is proportional to the difference between the index of that pixel and the index of the center pixel. We will refer to this pattern as the "raw pattern", see Fig. 3.

This report describes an extension of the algorithm to the more general case where several parallel, rigid lines are acquired at the same time. Also, the pixels on a scan line are distributed such that the (nominal) distance between two of them is proportional to the difference between the indices. We will refer to this pattern as the "system pattern", see Fig. 3. Thus, two kinds of pixel arrangements on a line are possible. We will, however, assume that all lines in a given image are arranged in the same way. In the latter case, the image has been "system corrected" prior to use of our algorithm.

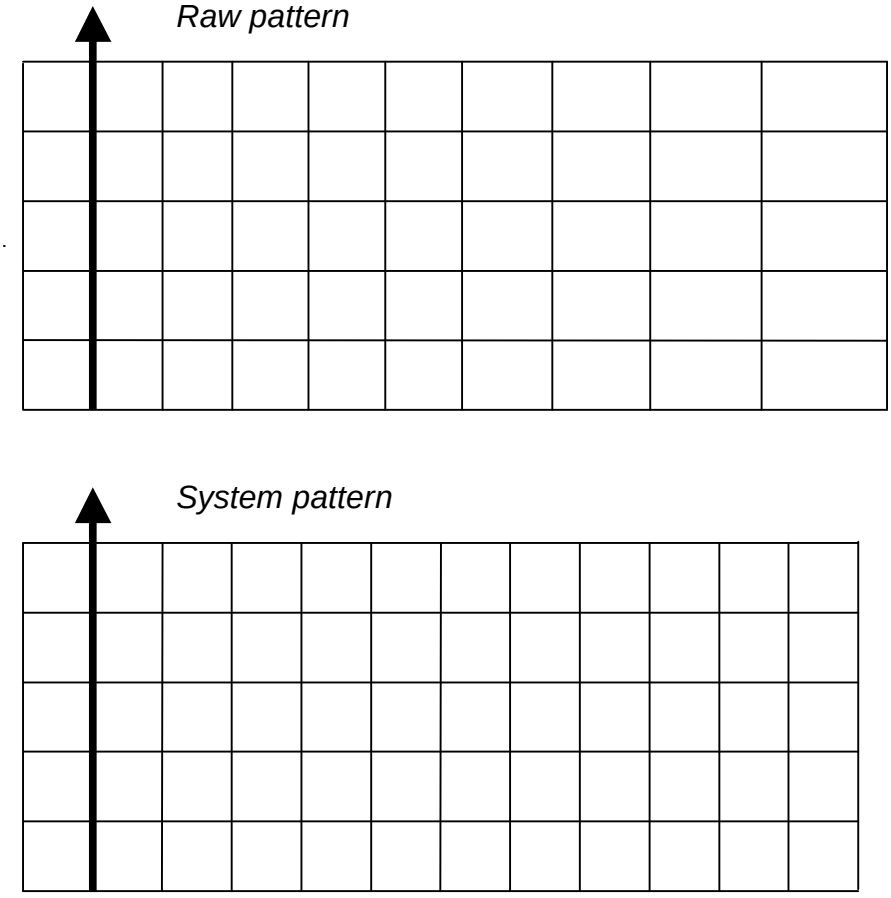

Fig 3. Arrangements of pixels (IFOVs).

The generalized algorithm is based on the same ideas as the original one. A Keplerian orbital model for the satellite motion is used, and by means of a set of ground control points, orbital parameters and satellite attitude are updated. Only longitude of ascending node and mean anomaly are adjusted as sufficiently accurate estimates of the remaining parameters are often available.

3.1. Updating the longitude of ascending node

The longitude of ascending node (Λ) is the first parameter to be updated. We exploit that for each ground control point (GCP), the following four geometric relations are valid (see Fig. 4):

$$\upsilon = \arcsin(\frac{r}{R}\sin\alpha) - \alpha \, .$$

$$\tan\delta = \frac{\sin\beta \;\; \sin\upsilon \;\; \cos\gamma}{\sin\Phi + \sin\upsilon \; \sin\gamma} \, .$$

$$\sin\Delta\lambda = \tan\Phi \, \tan(\delta + \gamma) \, .$$

$$\Lambda = \Delta\lambda + \lambda + \rho\,\Delta t \, .$$

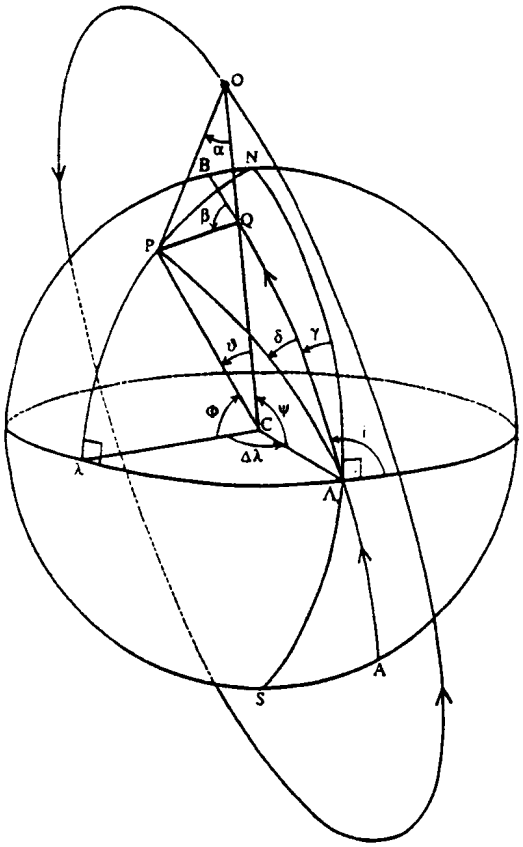

Fig. 4. Angles considered to define the satellite trajectory and viewing geometry for each observed GCP (AB = on-ground projection of the orbital trajectory). (The figure is taken from [1].)

The following notation is used: Φ and λ are the latitude and the longitude, respectively, of the GCP. υ is the angle between Earth's center – GCP and Earth's center – satellite. r is the satellite - Earth's center distance. R is the Earth's radius at the GCP. α is the angle between satellite - GCP and satellite - Earth's center. β is the angle between the ground track and the scan line. $\gamma = i - \frac{\pi}{2}$, where i is the inclination. δ is the angle between the orbital plane and the plane containing the Earth's center, the GCP, and the ascending node. $\Delta\lambda = \Lambda - \lambda$. ρ is the Earth's rotation rate. Δt is the difference between the time the GCP was imaged and the time the center of the image was acquired.

The minor and the major axes of the orbit yield lower and upper bounds for r, respectively. From the four geometric relations above, we deduce similar bounds for υ, δ, $\Delta\lambda$, and Λ. Thus, for each GCP, we have an interval containing Λ. Taking the midpoint of the intersection of these intervals yields a new estimate of Λ.

In the original algorithm, it is assumed that $\beta = \pi / 2$. However, this is not always true if several lines are acquired at the same time. In the general case, let l be the index of the line corresponding to the GCP, and let l_c be the index of the central line acquired at the same time. (l_c is not an integer if an even number of lines are acquired at the same time.) Let p be the pixel number of the GCP, and let p_c be the index of the center pixel.

If $l = l_c$, we have $\beta = \pi / 2$. Otherwise, $\beta = \arctan(d(p, p_c) / d(l, l_c))$, where $d(p, p_c)$ is the distance between GCP and the center pixel, and $d(l, l_c)$ is the distance between GCP and the central line. The distance $d(p, p_c)$ depends on the way the pixels are arranged on the scan line, while $d(l, l_c) = (l - l_c)\Delta y$, where Δy is the distance between two neighboring scan lines on the ground.

3.2. Updating mean anomaly

Concerning mean anomaly (M), we exploit that the discrepancy between the actual line number (l_T) of a ground control point and the predicted line number (l_P) from the model is mainly due to the deviation of the initial estimate of M from the true value. We let

$$M_{new} = M_{old} + \frac{2\pi \Delta y}{L_G} \sum (l_P - l_T)$$

where M_{old} and M_{new} are, the initial and the updated estimates, respectively, L_G is the length of the ground track, and the sum is taken over all GCPs.

The algorithm has a routine that calculates the line number of a point from its coordinates using a model of the situation of the image acquisition. The routine uses an array containing three vectors for each time instant data is acquired. These three vectors are the satellite's position, a unit vector perpendicular to the scanning plane (pointing roughly in the same direction as the velocity vector) and a unit vector

pointing from the satellite towards the first pixel of the corresponding image line, see Fig. 2. The algorithm also has a routine that builds up this array. How this is accomplished will be described later.

3.3. Adjustment for attitude effects

After updating the orbital parameters, the attitude angle of the satellite is considered. The following two fundamental vectors are introduced: $\vec{n}$ is the vector normal to the instantaneous scanning plane and $\vec{x}_1$ the viewing-direction vector of the first pixel of the corresponding scan line. Both vectors have unit length. For each GCP we determine $\vec{n}$ and $\vec{x}_1$. These two vectors are then adjusted according to attitude effects.

We show how to compute $\vec{n}$ and $\vec{x}_1$. For each GCP we know the time instant when the corresponding pixel in the image was seen by the satellite. At that time instant we compute the position of the satellite. Knowing the position we can calculate the nominal pointing direction ($\vec{q}$) which is defined to be the local (geodetic) vertical. $\vec{n}$ is found by normalizing $\vec{q} \times (\vec{v}_S \times \vec{q})$, where $\vec{v}_S$ is the velocity of the satellite, while $\vec{x}_1$ is found by rotating $\vec{q}$ an angle θ_1 around $\vec{n}$.

Determining the vector $\vec{w}$ (that is, the direction of the instantaneous gyro vector that accounts for attitude angle variations) and the angle σ introduce attitude effects. $\vec{w}$ and σ are estimated from relations based on the GCPs. The basic transformation that accounts for attitude angle effects is based on the determination of two vectors for each GCP: The "true" satellite position-observed point vector $\vec{r}_1$ and the "nominal" satellite position-observed point vector $\vec{r}_2$. $\vec{r}_1$ is given by normalizing $\vec{p} - \vec{s}$, where $\vec{p}$ is directly determined from the geographical coordinates of the GCP, and $\vec{s}$ is the position of the satellite. $\vec{r}_2$ is found by normalizing $c_x \vec{x} + c_n \vec{n}$, where $\vec{x}$ is found by rotating $\vec{q}$ an angle θ around $\vec{n}$. The coefficients c_x and c_n are given by

$$c_x = \frac{h}{\cos\theta},$$

$$c_n = (l - l_c)\,\Delta y,$$

where h is the satellite's altitude. The gyro direction is given by normalizing the vector product $\vec{r}_2 \times \vec{r}_1$, and the gyro angle σ around the direction $\vec{w}$ is given by $\arccos(\vec{r}_1 \cdot \vec{r}_2)$. The vectors are then adjusted by rotating an angle σ about $\vec{w}$.

After determining $\vec{n}$ and $\vec{x}_1$ for each time instant corresponding to a ground control point, we must determine $\vec{n}$ and $\vec{x}_1$ as continuous functions of time. For each component, a least-squares algorithm fits a second-degree polynomial in time. Having determined these six polynomials, a state table is created containing, for each time instant, the satellite's position, a unit vector perpendicular to the scanning plane and a unit vector pointing from the satellite towards the first pixel of the corresponding image line.

3.4. Calculation of a point's position in the original image

We are now ready to describe the routine that calculates the line number and the pixel number of a point from its geographical coordinates using a model of the situation of the image acquisition. The scanning time of the point is found by solving the equation $\vec{n}(t) \cdot \vec{r}_{SP}(t) = 0$, where $\vec{r}_{SP}$ is the vector from the satellite to the point. This is done by using a bisection method on the time interval between the first and the last scanning times of the image. At first, the bisection is performed on the data in the state table itself to find the two time instants (t_k and t_{k+1}) between which the expression $\vec{n}(t) \cdot \vec{r}_{SP}(t)$ changes sign. Then, a few more iterations are performed on the time interval between these two instants using linear interpolation to determine the values of the vectors. Let τ be the approximate solution, and let

$$m = \frac{\tau - t_k}{t_{k+1} - t_k}.$$

The line number of the central line acquired at t_k is given by $l_c(t_k)$. The line number (l) corresponding to the input point of the routine is then given by

$$l = l_c(t_k) + (l_c(t_{k+1}) - l_c(t_k))m.$$

$\vec{n}(t)$, $\vec{x}_1(t)$, and the satellite's position are also needed in the calculation of the pixel number. However, since several lines may be acquired at the same time, the number m used in the linear interpolation is modified. This ensures that the vectors are the same for all lines acquired at the same time, except for the areas between neighboring lines acquired at different time instants. We need the angle $\hat{\alpha}$ given by

$$\hat{\alpha} = \arctan\left(\frac{(\vec{n} \times \vec{x}_1) \cdot \vec{r}_{SP}}{\vec{x}_1 \cdot \vec{r}_{SP}}\right),$$

where $\vec{n} = \vec{n}(t_k) + (\vec{n}(t_{k+1}) - \vec{n}(t_k))m$, $\vec{x}_1 = \vec{x}_1(t_k) + (\vec{x}_1(t_{k+1}) - \vec{x}_1(t_k))m$, $\vec{r}_{SP} = \vec{p} - \vec{s}$, $\vec{p}$ is the point, and $\vec{s}$ is the position of the satellite. $\vec{s}$ is given by $\vec{s} = \vec{s}(t_k) + (\vec{s}(t_{k+1}) - \vec{s}(t_k))m$. If the pixels on a scan line are distributed according to the "raw pattern", the pixel number is given by $1 + const \cdot \hat{\alpha}$. If the distribution follows the "system pattern", the pixel number is given by

$$p_c + \frac{h}{\Delta x}\tan(\theta_1 + \hat{\alpha}).$$

Using this routine the line number and the pixel number in the input image can be determined from a pixel in the corrected output image. Since these numbers are not necessarily integers resampling is performed. Both nearest neighbor and bilinear interpolation are implemented.

4. Automatic detection of control points

In order to use the correction algorithm, locating the GCPs in the raw images is important. This is done by an automatic algorithm, [2]. In addition to the raw image, a digitized reference image correctly registered to the desired map projection is input to the algorithm. Water masks may replace these images. In this section, we describe briefly the method on which the algorithm is based.

Around each GCP a provisionally corrected sub-image is created. This is done by a modification of the correction algorithm described in the previous sections. The modification consists of omitting the parts involving the GCPs. That is, the original orbital elements (and not the updated ones) are used in the model, and attitude variations are ignored. A GCP is then located by establishing a correspondence between the provisionally corrected sub-image and the reference image. The correspondence is found by matching the two images. The matching is performed by computing the sum

$$\sum_{(x,y)\in C} \left| c(x,y) - s(x+\Delta x, y+\Delta y) \right|$$

for points $(\Delta x, \Delta y)$ on a square K. In the expression, C is a subset of the reference image centered at the true location of the GCP, $c(x,y)$ and $s(x,y)$ are the pixel values at (x,y) of the reference image and the image to be corrected, respectively. When the point $(\Delta x, \Delta y)$ that minimizes the sum above is found, the image of a small surrounding square K' is magnified by means of interpolation. Similarly, a small subset C' of C centered at the true location of the GCP is magnified, and a search for the best match is performed. Thus the correspondence is determined by sub-pixel accuracy. Input parameters to the algorithm specify the number of sub-pixels within a pixel and the dimensions of the sets K and K'.

It may happen the location of some of the GCPs obtained by the matching method is wrong. Such errors should be discovered. The location of the GCPs can be predicted from the model. It turns out that the discrepancy between the matched location and the predicted location is almost the same for each correctly detected GCP for a given image. Thus, if the discrepancy differs greatly from this, the matched location is likely to be wrong. In such cases, the location determined by the matching procedure should be rejected and replaced by an estimate based on the predicted location. The process of discarding matched locations goes as follows: In the first step, the average difference vector between predicted and matched locations is calculated. In the next step, the GCP with difference vector furthest from the average is found. If the Euclidean distance between the difference vector of the point and the average is greater than a tolerance limit ε, the point is rejected. These steps are repeated until either all the points satisfy the condition on the position relative to the predicted location, or there are only two points left.

5. Landsat TM data

A Landsat TM data set has been used to investigate the correction algorithm. Such images have seven bands, six of which have a pixel size of approximately 30 m $\times$ 30 m. The pixel size of the sixth band is 120 m $\times$ 120 m. The satellite's motion causes the extent of the image in one direction, while the view across the track is due to an oscillating mirror with its axis parallel to the velocity. The TM acquires sixteen lines for six of the bands during each mirror oscillation. For the last band, four lines are acquired during each mirror oscillation.

The image used here is obtained from SSC Satellitbild in Sweden. The image is not a raw image but "system-corrected". According to SSC Satellitbild this means that the following effects are accounted for:

- forward/reverse alignment,
- detector placement and delay,
- mirror scan profile,
- line length information,
- gyro data,
- angular displacement sensor data,
- attitude correction system data,
- ephemeris data,
- scan gap,
- Earth rotation,
- sensor altitude, and
- panoramic distortion.

Neither ground control points nor a digital terrain model has been used in the geometric correction. 27 files contain the image and additional information. The files are of nine different types. Seven of the files (one for each band) are leader files and contain scene identification, mission parameters, sensor parameters, processing parameters, and processed scene-related data like scale of processed inter-pixel distance and scale of processed inter-line distance. Seven files (one for each band) are imagery files that contain the image data and the time at start of each scan. One file is a supplemental file and contains input scene start time as well as ephemeris and attitude data. The remaining files do not seem to contain any information of interest to us. An algorithm that extracts the relevant information from the files and creates an image in the BIFF-format, [3], has been written.

6. Experiments

6.1. Landsat TM experiment

Data and input parameters

The algorithms have been tested on a system corrected Landsat 5 TM image covering a part of Southern Norway including Jotunheimen and Heimdalen test site used in SNOWTOOLS. The image was acquired on June 5th 1997 under sunny conditions. 18 ground control points were selected, see Table 1 and Fig. 5.

In order to detect these GCPs we used water masks obtained from the Norwegian Mapping Authority (Statens kartverk) as a reference image. The water masks are shown in Fig. 6, A1-A18. As input image we used a mask image derived from the Landsat TM image rather than the Landsat TM image itself. This mask image was produced in order to extract water bodies by thresholding the near-infrared band since water has almost zero reflectance in that band. The threshold value is 10.

When running the GCP detection algorithm, some input parameters were set. The sub-image C contained 151×151 pixels and the side length of the square K was 3 km. Moreover, the sub-image C' contained 3×3 pixels while the side length of the square K' was 60 m. The magnification factor was 10, and the tolerance limit ε was equal to 300 m. For definitions of ε and the sets C, C', K, and K', see Section 4.

Throughout the experiments the altitude of the satellite was set equal to 705.3 km, which is the nominal satellite altitude, [4].

Results

Subsets of the search areas containing the detected GCPs are shown in Fig. 6, B1-B18. The algorithm rejected GCP no. 8. This is reasonable since the point that was found by the algorithm (Fig. 6, B8) appears to be far from the true location (Fig. 6, A8). The misdetection is due to the fact that the shape of the lake in the reference image is quite different from the shape of the area that is classified as water in the Landsat image. In the southwestern part of the lake, there is a region that was not classified as water. In this region, the pixel values in band 4 are typically between 40 and 50. We do not know the cause for this, but we believe it is the presence of ice.

We also see that the shape of the lake in A16 is completely different from the shape of the area that is classified as water in B16. Most of the pixel values in the region corresponding to the lake are between 10 and 20, and consequently, these pixels are not classified as water. Again we believe that this is due to ice. Despite this discrepancy, the location of GCP no. 16 determined by the algorithm appears to be close to the true location. By inspecting the other B-images and comparing with the corresponding A-images in Fig. 6, we see that the automatic detection algorithm worked reasonably well.

Table 1. Location and altitude of ground control points.

GCP NO	NAME	UTM EAST	UTM NORTH	ALTITUDE (meters)
1	Lærdalsfjorden/Årdalsfjorden	412460	6780250	0
2	Lusterfjorden	424990	6818670	0
3	Fagernes	512690	6760780	353
4	Ringsjøen	573080	6750840	397
5	Randsfjorden	567110	6738720	134
6	Årdalsvatn	431238	6790612	0
7	Vågåvatn	493490	6858020	362
8	Tesse	499490	6845020	851
9	Vangsmjøsa	479020	6779130	464
10	Helin	484960	6764550	868
11	Slidrefjorden	498020	6772870	364
12	Furusjøen	537690	6848720	840
13	Atnsjøen	558810	6861640	696
14	Harsjøen	606340	6858050	680
15	Lomnessjøen	614990	6850020	258
16	Reinsvatnet	587520	6788820	905
17	Mjøsa I	578010	6775520	122
18	Mjøsa II	582490	6764790	122

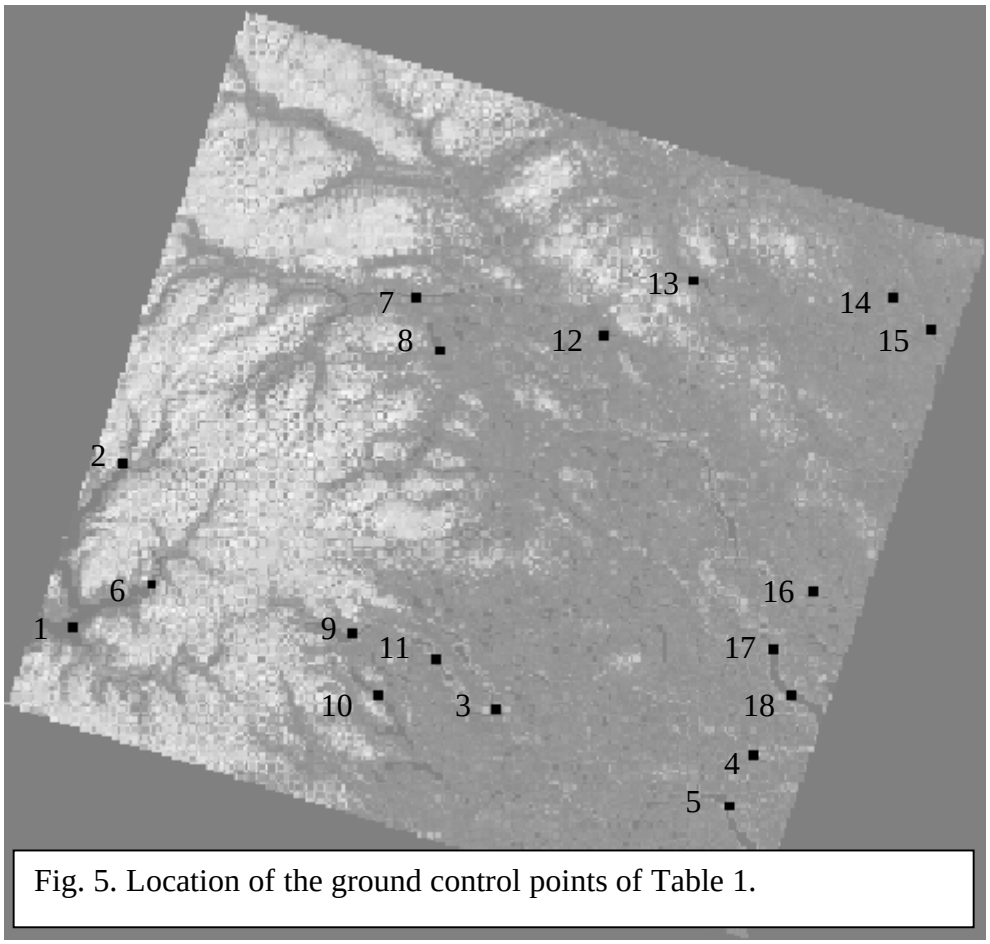

Fig. 5. Location of the ground control points of Table 1.

A1

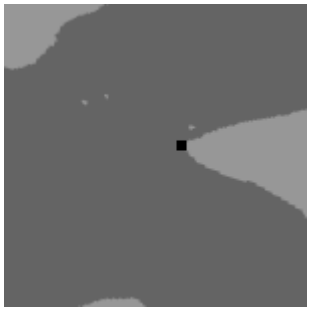

B1

C1

A2

B2

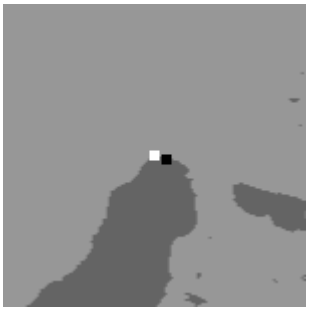

C2

A3

B3

C3

A4

B4

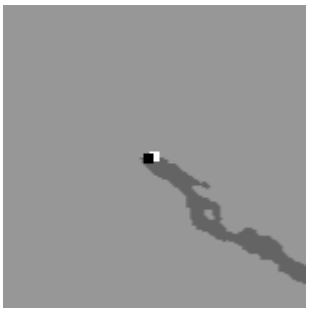

C4

A5

B5

C5

A6

B6

C6

A7

B7

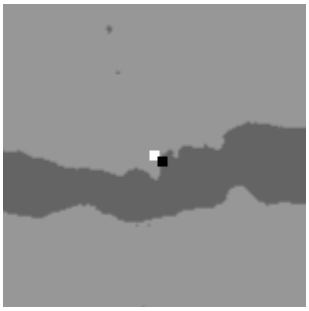

C7

A8

B8

A9

B9

C9

A10

B10

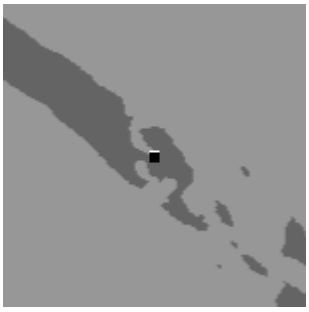

C10

A11

B11

C11

A12

B12

C12

A13

B13

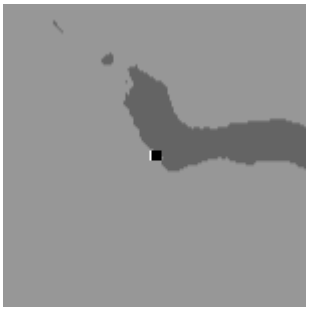

C13

A14

B14

C14

A15

B15

C15

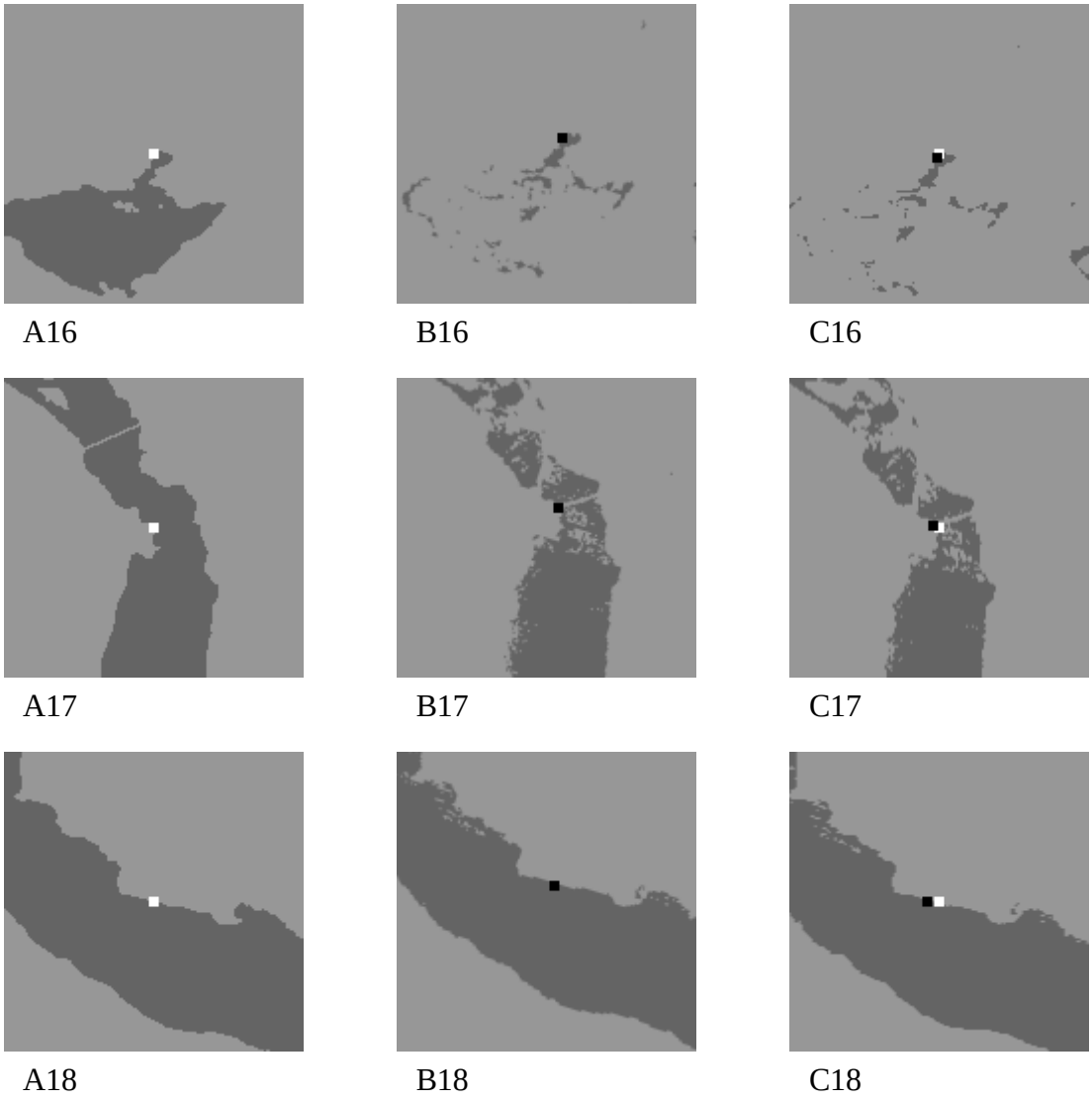

Fig. 6. Ground control points. A1-A18 show sub-images of the reference image centered at the ground control points (white marks). B1-B18 show sub-images containing the detected GCPs (black marks). C1-C18 show sub-images of the corrected image containing the GCPs. The white marks indicate the true locations, while the black marks indicate the location in the corrected image. If the distance between the two locations is short the white mark is (partially) occluded. The size of the marks correspond to 150 m $\times$ 150 m in the terrain.

Table 2. Estimates of orbital parameters.

ORBITAL PARAMETER	**INITIAL ESTIMATE**	**UPDATED ESTIMATE**
Semi major axis (km)	7066.554	
Eccentricity	0.001793	
Inclination (degrees)	98.3060	
Argument of perigee (degrees)	35.3608	
Longitude of ascending node (degrees)	173.8174	173.8166
Mean anomaly (degrees)	81.1050	81.1081

We then ran the correction algorithm using the GCPs found by the detection algorithm. The initial and updated estimates of the orbital elements are shown in Table 2. Fig. 7 shows a combination of bands 1-3 of the original system-corrected image and the resulting image registered to the UTM zone 32 projection is shown in Fig. 8. By the first glance at the image the result looks appealing. The main features like Sognefjorden, Mjøsa, and Randsfjorden are found at expected locations. Fig. 6, C1-C18, shows thresholded sub-images containing the GCPs. We have omitted GCP no. 8 since this point could not be detected properly. We see that the location of GCP no. 1, 2, 6, and 7 in the image are shifted to the east of the true location, while the location of GCP no. 5 and 18 in the image are shifted to the west of the true location. Concerning the remaining GCPs, the errors are smaller.

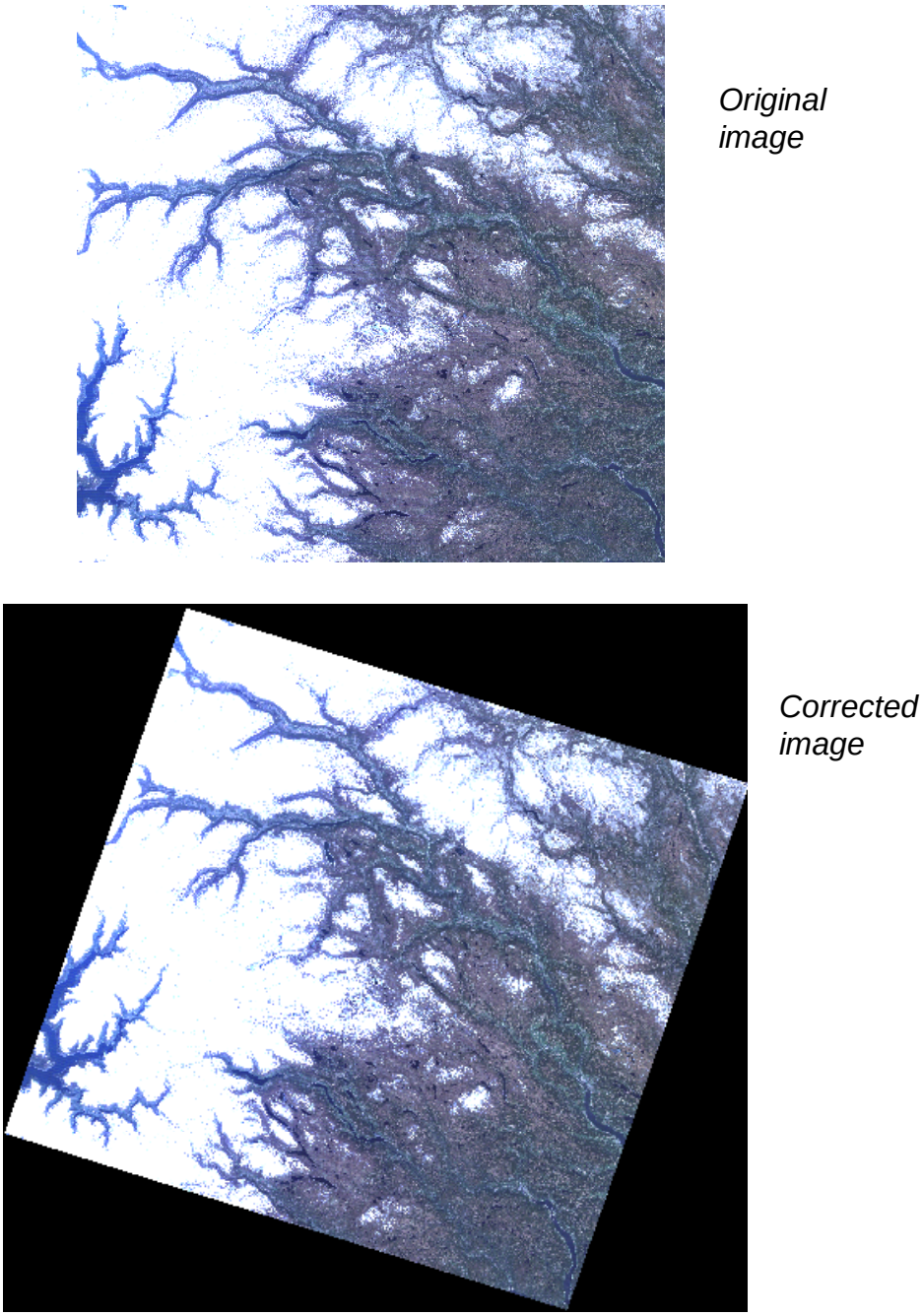

Original image

Corrected image

Fig 7. A combination of bands 1-3 for the original image and the corresponding corrected image obtained by the algorithm.

Quantification of errors

In order to quantify the errors, we employed the following procedure: For each accepted GCP we ran the detection and the correction algorithms without using that GCP. Then, by using the obtained mapping from the corrected image to the original image the location of the GCP in the original image was found. The difference and the distance between this location and the corresponding location found by the detection algorithm were computed. A summary of the results is given in Table 3.

We observe that the error in the across track direction is higher that the error in the along-track direction. For GCP no. 1, 2, and 6, which are the GCPs located furthest to the west of the ground track, and for GCP no. 5 and 18, which are among the GCPs located furthest to the east of the ground track, we see that the distance to the ground track is overestimated by more than five pixels. For GCP no. 3, 8, 9, 10, 11, 12, and 13, which are closer to the ground track, the error is smaller. The root mean square error is 4.3 pixel units, that is 129 m. The rightmost columns of Table 3 show that the errors become slightly smaller when all the GCPs are employed in the correction procedure. Then the root mean square error is 3.6 pixel units, that is 108 m.

Table 3. Summary of the results for Landsat TM data. Δx and Δy are the errors in pixel units in the across and along track directions, respectively. The distance is equal to $\sqrt{(\Delta x)^2 + (\Delta y)^2}$.

	Errors when GCP is not used			**Errors when GCP is used**		
GCP no.	**Δx**	**Δy**	**distance**	**Δx**	**Δy**	**distance**
1	–6.1	0.7	6.1	–4.4	0.7	4.5
2	–8,5	1.2	8.6	–7.3	1.2	7.4
3	1,4	–1.3	1.9	1.2	–1.3	1.8
4	3.5	0.0	3.5	3.0	0.0	3.0
5	5.9	–0.6	6.0	4.9	–0.6	4.9
6	–5.9	1.1	6.0	–5.3	1.1	5.4
7	–6.3	1.2	6.4	–5.2	1.2	5.4
9	–1.9	–0.2	1.9	–1.7	–0.2	1.7
10	–0.9	–0.5	1.0	–0.7	–0.5	0.8
11	0.4	–0.8	0.9	0.3	–0.3	0.4
12	–1.9	0.3	2.0	–1.7	0.3	1.8
13	–0.5	0.9	1.1	–0.6	0.9	1.1
14	–0.4	–0.1	0.4	–1.3	–0.1	1.3
15	1.3	–1.0	1.6	0.4	–1.0	1.1
16	2.0	–1.7	2.6	0.8	–1.2	1.5
17	3.9	1.2	4.1	3.2	1.2	3.5
18	5.5	–1.0	5.6	4.8	–1.0	4.9
MEAN/RMS	–0.5	0.0	4.3	– 0.6	0.0	3.6

6.2. Semi-MODIS experiment

We have also tested the correction procedure on an image with 240 m $\times$ 240 m pixels, which is about the pixel size of EOS MODIS' short wavelength bands. The image is obtained by resampling the Landsat TM image used in Section 6.1. We used the same 18 ground control points as in Section 6.1, see Table 1 and Fig. 5. The reference images, which were used in order to detect the GCPs, were obtained by resampling the reference images of Section 6.1. As in Section 6.1, the input image to the detection algorithm was produced by thresholding the near-infrared band, and the threshold value is 10. When running the GCP detection algorithm, some input parameters were set. The sub-image C contained 17×17 pixels and the side length of the square K was 4.8 km. Moreover, the sub-image C' contained 3×3 pixels while the side length of the square K' was 480 m. The magnification factor was 10, and the tolerance limit ε was equal to 600 m. For definitions of ε and the sets C, C', K, and K', see Section 4.

Quantification of errors is done by the same method as in Section 6.1. A summary of the results is given in Table 4. We observe that the error in the across track direction is higher that the error in the along track direction. The root mean square error is 0.9 pixel units. If all the GCPs are employed in the correction procedure, the root mean square error is as small as 0.7 pixel units.

Table 4. Summary of the results for the Semi-MODIS experiment. The errors are measured in pixel units.

	Errors when GCP is not used			**Errors when GCP is used**		
GCP no.	**Δx**	**Δy**	**distance**	**Δx**	**Δy**	**distance**
1	–0.4	0.9	1.0	–0.3	0.7	0.7
2	–0.8	0.5	1.0	–0.7	0.4	0.8
3	0.1	–0.8	0.8	0.0	–0.7	0.7
4	1.5	–0.1	1.5	1.1	–0.1	1.1
5	0.5	0.1	0.5	0.4	0.0	0.4
6	–0.9	0.2	0.9	–0.8	0.1	0.8
7	–1.2	–0.1	1.3	–1.0	–0.1	1.0
9	–0.9	0.5	1.0	–0.8	0.5	0.9
10	–0.4	–0.2	0.5	–0.3	–0.2	0.4
11	0.3	–0.8	0.9	0.3	–0.8	0.8
12	–0.2	0.7	0.7	–0.2	0.6	0.6
13	0.0	–0.8	0.8	–0.1	–0.7	0.7
14	–0.4	0.5	0.6	–0.6	0.3	0.7
15	1.3	0.1	1.3	0.7	0.1	0.8
16	1.0	0.4	1.1	0.4	0.3	0.5
17	–0.1	0.2	0.2	–0.2	0.2	0.3
18	0.9	–0.6	1.1	0.8	–0.5	0.9
Mean/RMS	0.0	0.0	0.9	–0.1	0.0	0.7

7. Discussion and conclusions

We have described a method for geometric correction of satellite images generalizing a method developed for NOAA AVHRR images. We have also presented an approach for automatic detection of ground control points. The methods have been tested on two images: a system-corrected Landsat TM image with pixel size 30 m $\times$ 30 m and a semi-MODIS image with pixel size 240 m $\times$ 240 m obtained from the system-corrected Landsat TM image by a resampling procedure. The detection procedure gave satisfying results. Using the correction method we obtained root mean square errors of 4.3 pixel units and 0.9 pixel units, respectively, for the two images. Moreover, the error in the across-track direction is higher than the error in the along track direction. However, we believe that it is possible to achieve higher accuracy.

Apparently, the distance to the ground track is overestimated. Furthermore, this error increases as the distance to the ground track increases. This suggests that the altitude value of the satellite employed in the experiments is too high. In fact, using an altitude of 704 km instead of 705.3 km gave a root mean square error of 1.7 pixel units on the Landsat TM image. Therefore, in further developments of the algorithm, an improved estimate of the altitude should be computed. This could be done in several ways. Firstly, the altitude of the satellite can be calculated by utilizing knowledge about its position. Secondly, an estimate can be obtained by minimizing the discrepancy between the predicted and actual locations of the GCPs with respect to the altitude.

When performing the correction, it was assumed that the altitude of each terrain point in the image was zero. This assumption was also made in the experiments reported in [2]. In that case, the resolution was as coarse as 1 km $\times$ 1 km and satisfactory results were obtained despite the simplification. In this case, however, the resolution is much finer, and the value of the altitude at the various points in the scene is more significant. Thus, utilizing a digital elevation model should be considered.

As in [2], only two of the orbital element estimates (longitude of ascending node and mean anomaly) were adjusted by using the GCPs. Since higher estimation accuracy is required here, it should be investigated whether an improvement of the other four orbital element estimates is fruitful.

In the correction method presented in this report, the vector normal to the instantaneous scanning plane and the viewing-direction vector of the first pixel of the corresponding scan line were modeled as second-degree polynomials in time. Other models, that may be more appropriate, could be investigated. However, a higher number of ground control points is needed if the number of unknown parameters in the models to be estimated is high.

So far, we have discussed possible improvements of the correction method. The method for automatic detection of GCPs may also be improved. In the experiments reported here, most of the GCPs were detected successfully. However, the image was acquired under almost ideal conditions due to the lack of clouds. If clouds are present, the task of detecting GCPs is more difficult, see [2] for further details.

In order to obtain satisfactory results, the GCPs must be carefully chosen. It is recommended that a GCP is located on a contour of a water body, which is not too small. Furthermore, the contour should be characteristic and identifiable. However, it happens that ice or snow covers a water body. Under such conditions, the method that detects a water body by thresholding band 4 of the Landsat TM image will not work. Consequently, the GCP may not be detected successfully. In this case, one may attempt to recover the water body by other means. If the water body is covered by ice it may be distinguished from its surroundings. If recovery is impossible or very difficult, the GCP should be rejected.

The main conclusion from the work presented here is that the improved automatic geometric correction algorithm represents an accurate method for correction of EOS MODIS data, but has to be improved for application to Landsat TM data. Since MODIS is a preferred sensor for remote sensing of snow (see [5]), the current results should be very valuable for operational applications. The same is true for the GCP-matching method based on water masks, which should be much more robust than applying traditional image-difference or correlation methods.

8. Acknowledgements

This work was supported by the European Union's Environment & Climate R&D Programme (contract no. ENV4 CT96-0304), Royal Norwegian Research Council, EnFO (Norway), Statkraft (Norway), and Norwegian Water Resources and Energy Administration (NVE).

9. References

[1] J.F. Moreno and J. Meliá: A Method for Accurate Geometric Correction of NOAA AVHRR HRPT Data, *IEEE Transactions on Geoscience and Remote Sensing*, Vol. 31, No. 1, pp. 204-226, January 1993.

[2] R. Solberg, S. Kolberg, O.M. Halck, H. Koren, and D. Vikhamar: *Integrasjon av satellittbasert snøkartlegging og hydrologisk modellering*, NR Rapport nr. 925, December 1997 (in Norwegian).

[3] S. Bøe, T. Lønnestad, and O. Milvang: *XITE User's Manual*, Report No. 56, Image Processing Laboratory, Department of Informatics, University of Oslo, June 1998.

[4] *The TELSAT Guide*, Available online: http://www.belspo.be/telsat/landsat/msax_003.htm, January 1995.

[5] R. Solberg, D. Hiltbrunner, J. Koskinen, T. Guneriussen, K. Rautiainen and M. Hallikainen, *Snow Algorithms and Products – Review and Recommendations for Research and Development*, Project SNOWTOOLS WP 410, NR Report No. 924, December 1997, Norwegian Computing Center, Oslo.

SNOWTOOLS Project Participants

Project Coordinator:
Tore Guneriussen
NORUT Information Technology Ltd.
9005 Tromsø, Norway
Phone: +47 776 29421
Fax:+47 776 29401
E-mail: tore.guneriussen@itek.norut.no

Contractors:
Martti Hallikainen
Helsinki University of Technology
Otakari 5 A, FIN-02150 Espoo
Finland
Phone: +358-9-451 237
Fax: +358-9-451 2898
E-mail: hallikainen@avanet.hut.fi

Andrew Harrison
University of Bristol
University Road
Bristol BS8 1 SS
UK
Phone:+44 117 9288303
Fax:+44 117 9287878
E-mail: a.r.harrison@bristol.ac.uk

Sjur Kolberg
SINTEF Civil and Environmental Engineering
N-7034 Trondheim
Norway
Phone: + 47 73 59 60 94
Fax:+47 73 59 02 01
E-mail: sjur.a.kolberg@civil.sintef.no

Christian Matzler
University of Bern
Sidlerstr. 5, CH 3012 Bern
Switzerland
Phone: +41 316 314589
Fax: +41 316 313765
E-mail: matzler@iap.unibe.ch

Rune Solberg
Norwegian Computing Center
Box 114 Blindern
N-0314 Norway
Phone: +47 22 85 25 00
Fax: + 47 22 69 76 60
E-mail: rune.solberg@nr.no